First-principles study of thin TiO_x and bulklike rutile nanowires

D. Çakır and O. Gülseren*
Department of Physics, Bilkent University, Ankara 06800, Turkey
(Received 8 August 2008; revised manuscript received 29 August 2009; published 24 September 2009)

We have systematically investigated structural, electronic and magnetic properties of very thin TiO_x ($x=1,2$) nanowires as well as bulklike (110) rutile nanowires by using the first-principles plane-wave pseudopotential calculations based on density functional theory. A large number of different possible structures have been searched via total-energy calculations in order to find the ground-state structures of these nanowires. Three-dimensional structures are more energetically stable than planar ones for both of the stoichiometries (i.e., $x=1,2$). The stability of TiO_x nanowires is enhanced with its increasing radius as a result of reaching sufficient coordination number of Ti and O atoms. All stoichiometric TiO_2 nanowires studied exhibit semiconducting behavior and have nonmagnetic ground state. There is a correlation between binding energy (E_b) and energy band gap (E_g) of TiO_2 nanowires. In general, E_b increases with increasing E_g. In TiO nanowires, both metallic and semiconductor nanowires result. In this case, in addition to paramagnetic TiO nanowires, there are also ferromagnetic ones. We have also studied the structural and electronic properties of bulklike rutile (110) nanowires. There is a crossover in terms of energetics, and bulklike nanowires are more stable than the thin nanowires for larger radius wires after a critical diameter. These (110) rutile nanowires are all semiconductors.

DOI: 10.1103/PhysRevB.80.125424 PACS number(s): 61.46.Km, 62.23.Hj, 73.22.−f, 75.75.+a

I. INTRODUCTION

Titania, TiO_2, exits in a number of different crystalline forms, such as anatase, rutile and brookite. Thermodynamically, rutile is the most stable phase under ambient conditions. Since, it is nontoxic and environmentally clean, and because of its cheap production and stability under illumination, titanium dioxide is widely used in many different technological applications including self-cleaning coatings, pigments, sunscreens, toothpastes, photovoltaics, photocatalysis and photoelectrochemistry.[1–3] Surface properties and surface structure is very important for most of these applications. Therefore, increasing the surface area by producing the titania nanoparticles and nanowires might be very crucial. In addition to this, novel properties due to the quantum size effect might arise from small diameter nanowires of titania. In recent years, one-dimensional (1D) TiO_x nanostructures[3] such as nanorods, nanowires, and nanotubes have been investigated extensively because of their size and morphology dependent structural, chemical and electronic properties. They lead to a significant number of technological applications including gas and humidity sensors,[4] dye-sensitized solar cells,[5,6] photovoltaics, and photocatalysis.[7]

TiO_2 nanowires[8–13] can be synthesized on TiO_2 surfaces or in zeolites. Blanco-Rey *et al.*[8] have obtained nonstoichiometric Ti_2O_3 quasi-one-dimensional metallic chains along the [001] direction of (1×2) reconstructed rutile surface. Naturally, semiconductor monatomic titania ($\cdots$Ti-O-Ti-O$\cdots$) chains is formed in Engelhard titanosilicate-4 (ETS-4) (Ref. 9) and 10 (ETS-10).[10] Individual chains are isolated from each other by an insulating silicate layer. Electrical transport measurement has been made for ETS-4 and a non-Ohmic behavior has been observed. Conductivity of these monatomic chains increases with increasing bias voltages. Recently, TiO_2 atomic wires with a few angstroms diameter are synthesized by solution methods.[13] Structural, electronic and vibrational properties of titania chains embedded in ETS-10 have been studied using *ab initio* methods.[14] Moreover, Enyashin *et al.*[15,16] have studied the stability and electronic structure of various TiO_2 nanotubes governed from anatase and lepidocricite layer modifications by using density-functional-based tight-binding method. Futhermore, *ab initio* calculations are reported that investigates atomic scale[17] as well as the rutile[18] TiO_2 nanowires.

Therefore, a thorough analysis of the structural and electronic properties of stoichiometric and nonstoichiometric titania nanowires is necessary before one aims at its possible applications. Our motivation in this work is to understand how thin TiO_x and rutile (110) nanowires are formed and their properties due to the dimensionality. This work presents a systematical investigation of structural, electronic and magnetic properties of these nanowires within the density-functional theory (DFT).

II. COMPUTATIONAL METHODS

Total-energy and electronic-structure calculations have been performed by first-principles plane-wave method[19,20] based on DFT (Ref. 21) using both ultrasoft[22] and projected-augmented-wave (PAW) (Refs. 23 and 24) pseudopotentials with electronic configurations $3p^6 3d^3 4s^1$ for Ti atoms and $2s^2 2p^4$ for O atoms. The exchange-correlation potential has been treated by generalized gradient approximation (GGA).[25] All structures have been represented in a tetragonal supercell geometry (with lattice parameters $a_{sc}=b_{sc}$ and c_{sc}) using periodic boundary conditions. To prevent interaction between adjacent isolated wires, a large spacing ($a_{sc}=b_{sc}\sim16$ Å) has been introduced. For single cell wire calculations, c_{sc} corresponds to lattice constant c and for double cell calculations $c_{sc}=2c$ (c being the lattice parameter of the TiO_x wires along the wire axis). Convergence with respect to the number of plane waves used in expanding Bloch functions and **k** points in sampling the Brillouin zone have been tested

TABLE I. Computed lattice constants a and c (in Å) and E_g (in eV) for anatase and rutile phases of bulk TiO_2. Ultrasoft pseudopotential results are presented. Very similar results are obtained by using PAW potentials. Experimental values are also shown for comparison. The lattice constants for rutile structure are from Refs. 28–30 and for anatase phase are from Refs. 29 and 30 while E_g data are from Refs. 37 and 38.

	Anatase			Rutile		
	a	c	E_g	a	c	E_g
Calc.						
GGA	3.81	9.76	2.30	4.64	2.98	1.90
LDA	3.75	9.50	2.22	4.57	2.94	1.93
Expt.	3.79	9.51	3.20	4.59	2.96	3.03

for each wire systems. A plane-wave basis set with kinetic energy cutoff $\hbar^2|\mathbf{k}+\mathbf{G}|^2/2m \leq 450$ eV has been used. In the self-consistent potential and total-energy calculations, Brillouin zone of nanowires has been sampled by $(1\times1\times27)$ and $(1\times1\times17)$ meshes in the k space within Monkhorst-Pack scheme[26] for single and double unit cells, respectively. In order to treat partial occupancies, Methfessel-Paxton smearing method[27] is used. The width of smearing has chosen as 0.08 eV for geometry relaxation and 0.01 eV for accurate energy band and electronic density of states calculations. All atomic positions and lattice parameters have been optimized by using conjugate gradient method where total energy and atomic forces are minimized. The convergence for energy has been chosen as 10^{-5} eV between two ionic steps, and the maximum force allowed on each atoms is 0.03 eV/Å.

III. RESULTS AND DISCUSSIONS

First of all, pseudopotential of Ti and O atoms have been tested. Calculated lattice parameters and energy band gap (E_g) of bulk rutile and anatase phases with two different exchange-correlation functionals [GGA and local-density approximation (LDA)] have been compared with available experimental data[28–30] in Table I. Due to pseudopotentials, exchange-correlation approximation and methods used in calculations, lattice parameters can be slightly different from both experimental[28–30] and previous calculated values.[31–34] The comparison of these results, similar to some recent studies[35,36] comparatively including several different exchange-correlation functionals as well as pseudopotentials suggests that GGA calculations yield slightly better agreement with experimental data. Hence, using GGA approximation, the calculated lattice parameters a and c of rutile are 4.64 (4.59) and 2.98(2.96) Å, respectively. The experimental values[28–30] are quoted in parentheses. For the case of anatase, a and c values are 3.81 (3.79) and 9.76(9.51) Å which are in fair agreement with experimental values.[29,30] Compared to the experimental data, maximum deviation appears with anatase c parameter (2.6%) while the variation in all the other lattice parameters from experimental values are less than 1%. E_g values are 1.90 (3.03) eV for rutile and 2.30 (3.2) eV for anatase. These gap values are smaller than the experimental values[37,38] which is a known deficiency of DFT calculations. In order to calculate correct gap values, it is necessary to go beyond standard DFT calculation by including self-interaction corrections such as GW calculations.

We have also checked the bond length in O and Ti dimer as well as TiO and TiO_2 molecules. O and Ti dimers have magnetic ground state and corresponding O–O and Ti–Ti bond lengths are 1.23 and 2.38 Å, respectively. TiO molecule prefers the magnetic ground state with magnetic moment value of $\mu=2\mu_B$ where Ti–O bond length is 1.63 Å (1.61 Å with LDA) in good agreement with experimental values.[39] Bent TiO_2 molecule is about 2 eV energetically more stable than linear one and both structures prefer the singlet state. Ti–O bond length and O–Ti–O bond angle are 1.66 Å and 109° (1.64 Å and 109° with LDA), respectively. Experimentally estimated value[40] of O–Ti–O angle is 110 ± 5. Ti–O–O–Ti structure is unstable in linear Ti_2O_2 molecule. Upon relaxation of linear Ti–O–O–Ti molecule, two separated Ti–O molecules resulted by breaking O–O bond. In Ti–O molecule, Ti atom donates two electrons to O atom. According to Hund's rule, remaining unpaired d electrons of Ti cause to magnetization in this molecule. In contrast to TiO molecule, Ti atom gives all the valance electrons to p orbitals of two O atoms in TiO_2 molecule. As a result of this charge transfer, TiO_2 is a closed shell molecule and has paramagnetic ground state.

A. $(TiO)_n$ nanowires

Several single and double stranded $(TiO)_n$ wires are investigated, and their optimized structures are presented in Fig. 1. Wire structures include both simple and more complicated structures together. In order to quantify the relative stabilities of these wires, binding energy E_b per formula unit (f.u.) for $(TiO)_n$ wires is calculated in terms of the total energy of wire, $E_T[(TiO)_n]$, and the energies of individual atoms, $E[Ti]$ and $E[O]$ for Ti and O atoms respectively, as,

$$E_b = E_T[(TiO)_n]/n - E[Ti] - E[O] \quad (1)$$

where n represents the number of TiO block in the unit cell. Variation in E_b with lattice constant c along the wire axis is shown in Fig. 2. It is noticed that there are two different regions along the energy axis in Fig. 2. First region is between −10 and −10.5 eV and related to the single stranded wires. Double stranded nanowires are observed in the second region which is approximately 1 eV lower in energy than the previous one. Along the series of single stranded wires, Ti atom is undercoordinated compared to the bulk structures, and coordination number is varied between one and three, depending on the structure. Remember that in bulk TiO_2, Ti and O atoms are sixfold and threefold coordinated, respectively. On the other hand, in double stranded systems which are more energetically stable, coordination number of Ti atoms becomes four. Therefore, we can infer that coordination number influences the strength of binding in these wires. In each region, three-dimensional (3D) wires (B6, B7, C3, C4) are more stable than planar (B1, B2, B3, B4, B5, C1, and C2) wire structures. Existence of monovalent O or Ti atoms

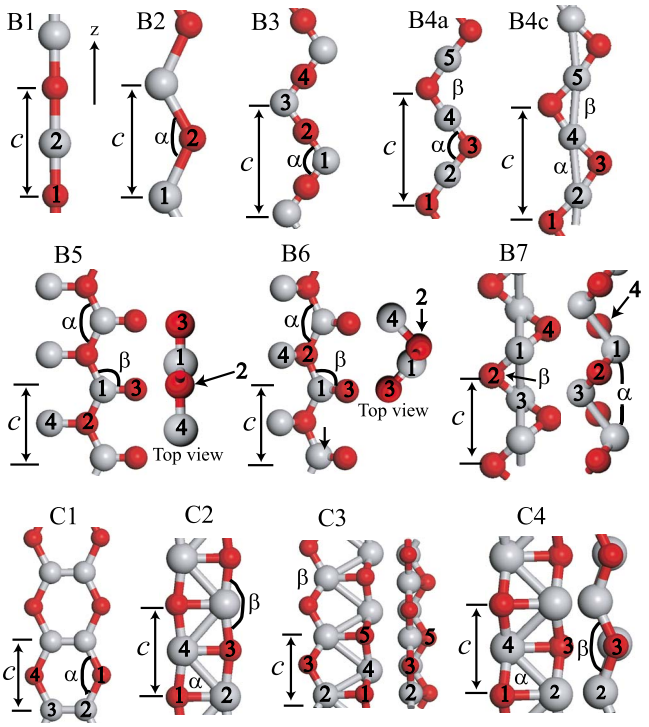

FIG. 1. (Color online) Optimized geometric structure of isolated $(TiO)_n$ nanowires. Assigned labels are indicated in order to identify each of the wire. Light (gray) and dark (red) balls are used to represent Ti and O atoms, respectively. Lattice constant c, distance between the numbered atoms and indicated angles α and β at equilibrium are compiled in Table II.

also affect the binding. B5 and B6 structures have both monovalent Ti and O atoms. Coordination number of these monovalent atoms is one. Formal oxidation states of Ti and

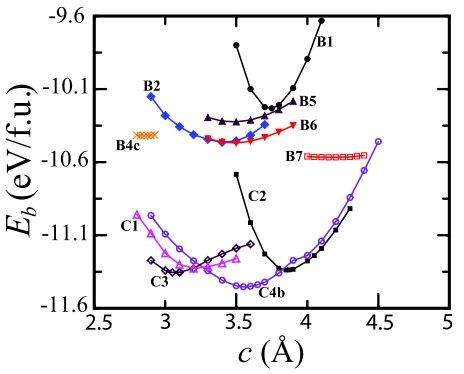

FIG. 2. (Color online) Variation in binding energy, E_b (eV/f.u.), with the lattice constant c in different $(TiO)_n$ wires. Lattice constant of B4c structures is multiplied by 0.5 in order to present all the data with a compact horizontal axis.

O atoms are (+4) and (−2), whereas in the structures with TiO units, formal oxidation states of Ti and O atoms are (+2) and (−2). As a result, these monovalent atoms are undercoordinated and these atomic sites might be very reactive against to adsorbate atomic and molecular species. For the double stranded wires, our initial starting geometry for structural minimization was planar, however for C3 and C4 wires planar structure is not preserved during the geometry optimization.

Lattice parameter along the nanowire axis, some bond angles and interatomic bond distances between the atoms labeled in Fig. 1, magnetic properties and E_b of $(TiO)_n$ wires at their ground states are summarized in Table II. Bulk titanium monoxide is also included in this Table for comparison. Bulk TiO crystal structure is α-TiO, that is a monoclinic phase which can be derived as ordered vacancies (~15%) from simple sodium chloride with formula Ti_5O_5.[41–43] Due

TABLE II. Optimized lattice constant c_0 (in Å), interatomic bond distances d_{1-2}, d_{1-3}, d_{2-3}, d_{1-4}, d_{2-4}, and d_{4-5} (in Å), angles α and β (in degree), and binding energies E_b (in eV/f.u.) of $(TiO)_n$ nanowires. Magnetic moment (μ) of the ferromagnetic wires are presented in terms of Bohr magneton μ_B.

Wire	c_0	d_{1-2}	d_{1-3}	d_{2-3}	d_{1-4}	d_{2-4}	d_{4-5}	α	β	E_b	μ
B1	3.7	1.85								−10.13	2
B2	3.4	1.83						136.6		−10.26	2
B3	6.6	1.84		1.84		3.30		128.0		−10.21	4
B4a	5.75	1.85		1.85		2.88	2.88	101.5	101.8	−10.21	2.47
B4b	5.75	1.85		1.86		2.9	2.85	102.6	100.7	−10.22	2.47
B4c	5.7	1.83		1.88		2.86	2.86	100.8	100.8	−10.22	2.47
B5	3.5	1.95	1.64			1.87		127.7	116.3	−10.12	2.87
B6	3.5	1.95	1.65			1.91		128	114.1	−10.27	2
B7	4.15	1.84	2.62	1.85				104.9	90.4	−10.37	
C1	3.2	1.82		2.70	4.44			122.8		−11.12	
C2	3.9	1.98	2.93	1.94		2.62		83.0	166.1	−11.14	
C3	3.1	2.00	3.31	1.84	1.93	2.78	2.81	67.4	115.2	−11.15	1.05
C4a	3.55	2.00	2.98	1.93		2.59		82.0	133.9	−11.16	2.19
C4b	3.55	2.02	2.99	1.91		2.54		80.6	136.1	−11.24	
α-TiO		2.00–2.13								−13.01	
Cubic TiO		2.14								−12.91	

to high coordination of atoms in bulk TiO compared to nanowires, interatomic bond distance between Ti and O atom is around 2.00–2.13 Å. Energy difference between the E_b of most energetically stable TiO nanowire studied here, C4b, and cohesive energy of bulk TiO is 1.77 eV.

More insight about the stability and bonding nature of these nanowires can be provided by examining three isomers of B4 structure. B4a is uniform B4 in which $d_{2-4}=d_{4-5}$. Next isomer is shaped by forming Ti–Ti dimers, so B4 nanowire gains very small energy (about 10 meV) with respect to the B4a structure. This structure is called B4b and $d_{2-4}\neq d_{4-5}$. Third isomer is B4c structure, in which B4 wire gains further energy upon formation of internal Ti zigzag chain. B7 structure can be obtained by compression of B4 chain. It can be easily seen from Fig. 1 or Table II that lattice constant of B3 chain is the largest. One of the O (Ti) atom in doubled unit cell of B2 is rotated 180° to obtain B3 (B4) structure. In other words, the B3 or B4 wires are formed by combining linear O–Ti–O units which have larger total energy than bent O–Ti–O units (see B2 structure). On the other hand, in B4 structure, repulsive O–O interaction is small relative to B3 wire. Hence, the lattice constant of B4 (B3) structure is very large compared to other single stranded wires in order to minimize repulsive O–O interaction that would compensate the energy loss due to the linear O–Ti–O units.

Most of the structures have magnetic ground state. However, in both single and double stranded wires, nonmagnetic wires (B7 and C4b) have the lowest energy. In C4 structure, energy difference between the magnetic (C4a) and nonmagnetic states (C4b) is 193.6 meV. Structural parameters of these magnetic and nonmagnetic isomers are not so different. B4 isomers have almost equal magnetic moment which is $\mu=2.47\mu_B$, while the related wire structure B3 has the largest magnetic moment, $4\mu_B$. Magnetic moment of B1 and B2 are $2\mu_B$. On the contrary, ground state of bulk TiO structure is paramagnetic.

In general, $(TiO)_n$ wires exhibit metallic behavior as seen in Fig. 3 while C1, C4b, B3 and B7 structures are semiconductor. Figures 3(a)–3(d) show the electronic band structure of double stranded wires whereas the ones of single stranded wires are collected in Figs. 3(e)–3(h). In the band structure of lowest energy structure, C4b, conduction band and valance band edges are very close to the E_F at Γ and Z points, respectively. E_g is 0.19 eV and has indirect nature for this nanowire. In most of the band structures, there are couple of bands below the Fermi level, E_F, and then a large band gap of a few eV's occurs. For example, in the electronic band structure of C4b wire shown in Fig. 3(d), there are two bands located just below the E_F before a band gap of approximately 4 eV, and they are occupied by 4 electrons. If we remove four electrons one by one from C4b wire, E_F goes down in energy in the calculated band structure of charged C4b nanowire, and eventually wire becomes a semiconductor. A similar situation happens for the other $(TiO)_n$ nanowires. Therefore, it is possible to infer that the stability of $(TiO)_n$ wires might be enhanced upon adsorption that yield a charge transfer from these wires. Interestingly, B6 exhibits half metallic behavior. While, this nanowire is metallic for the spin up electrons, it is an indirect band-gap semiconductor with a E_g of 0.74 eV for spin down electrons.

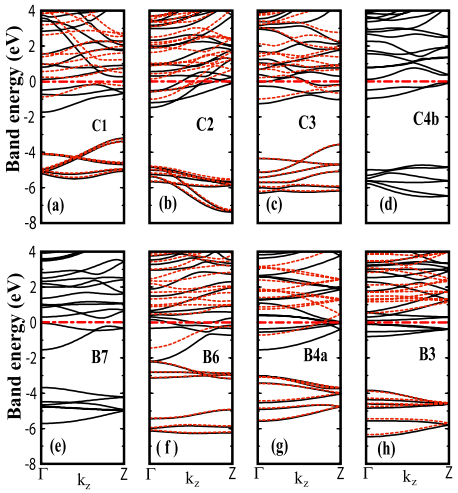

FIG. 3. (Color online) The band structure of the selected $(TiO)_n$ wires. Fermi level of metallic systems shown by dashed lines mark the zero of energy. For magnetic systems, majority (minority) spin components are represented with dark solid (orange dashed) lines.

B. $(TiO_2)_n$ nanowires

A large number of different possible initial wire geometries have been optimized by conjugate gradient minimizations in order to find the ground-state structures of $(TiO_2)_n$ nanowires. Total energy of these structures is minimized with respect to lattice constant along the wire axis as well. Optimized nanowire geometries are presented in Fig. 4. Similar to the TiO wires, E_b per f.u. of $(TiO_2)_n$ wires have been calculated in terms of the total energy of wire, $E_T[(TiO_2)_n]$, and the energies of individual atoms, $E[\mathrm{Ti}]$ and $E[\mathrm{O}]$ for Ti and O atoms, respectively, as,

$$E_b = E_T[(TiO_2)_n]/n - E[\mathrm{Ti}] - 2E[\mathrm{O}] \quad (2)$$

where n is the number of TiO_2 block in the unit cell. E_b versus lattice constant c along wire axis is illustrated in Fig. 5.

Lattice parameter along the nanowire axis, bond angle and interatomic bond distances between the atoms labeled in Fig. 4, binding energy E_b, and energy band gap E_g of $(TiO_2)_n$ wires at their ground states are summarized in Table III. The stability and possibility of formation of TiO_2 nanowires can be investigated by comparing E_b of these nanowires with that of bulk phases of TiO_2. It is known that rutile phase of titania is thermodynamically more stable than anatase phase. E_b per f.u. for rutile phase is −20.51 eV. The binding energy with respect to the cohesive energy of bulk rutile phase, E_b^r, might be defined as $E_b^{wire}-E_b^{rutile}$. Here, E_b^{wire} and E_b^{rutile} are the binding energies of an isolated nanowire and rutile bulk titania. E_b^r is also included in Table III. $E_b^r>0$ means that bulk rutile is more stable than a particular wire structure. It is observed that E_b^r is positive for all TiO_2 nanowires. But in our calculations, the total energy, not the free energy of these phases has been calculated.

The A1 and A2 wires have related structures. In a double cell of A1 geometry, one of the low-coordinated O atoms is rotated by 180° with respect to the other low-coordinated O atom to obtain the A2 structure. Difference between E_b's of

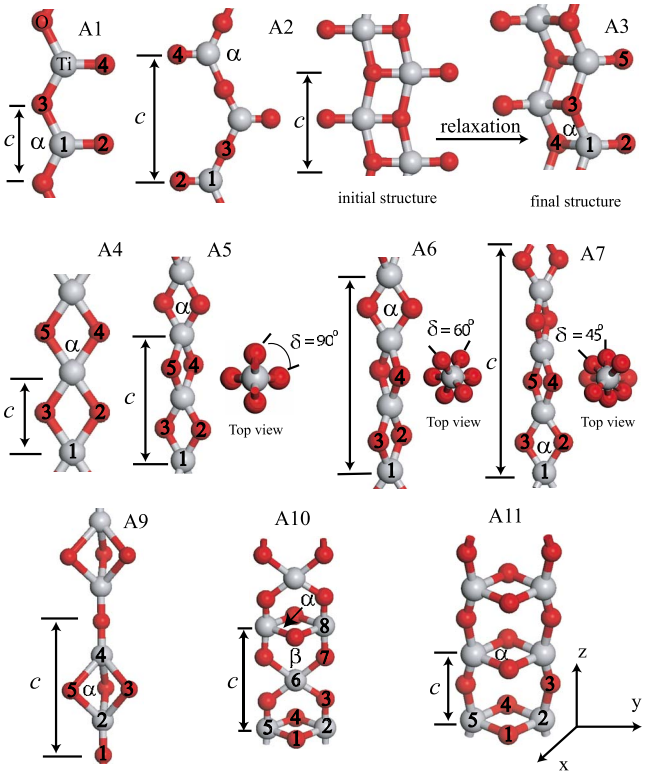

FIG. 4. (Color online) Atomic structure of isolated $(TiO_2)_n$ wires. Assigned labels are indicated in order to identify each of the wire. Light (gray) and dark (red) balls are used to represent the Ti and O atoms, respectively. Lattice constant c, distance between the numbered atoms and indicated angle α at equilibrium are summarized in Table III.

these two structures increases (decreases) when lattice constant decreases (increases). For larger lattice constants, interaction between the two low-coordinated O atoms decreases in the A1 structure. As a result, E_b's of A1 and A2 begin to get closer to each other. The difference between E_b's of A1

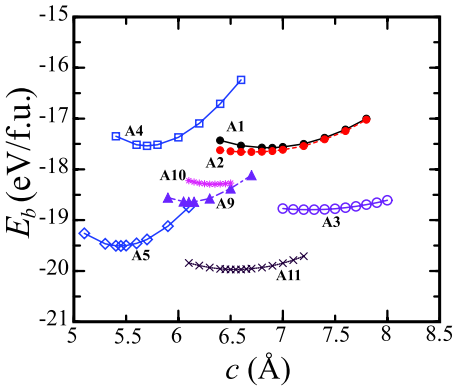

FIG. 5. (Color online) Variation in E_b (eV/f.u.) with respect to the lattice constant c along the wire axis in different $(TiO_2)_n$ nanowire structures. Lattice constant of A1, A3, A4, and A11 structures are multiplied by 2 in order to present all the data with a compact horizontal axis.

and A2 geometries at equilibrium is 168.6 meV. The distance between adjacent O atoms affects the stability of wires. O atom prefers to make its coordination at least two. A1 and A2 wires have monovalent O atoms. Relative stability of these isomers is reduced by these monovalent atoms. Ti–O bond length (d_{1-2}) between monovalent O and the nearest Ti atom is 10% shorter than other nearest-neighbor bond distances as seen in Table III.

A double strand wire is formed by combining two A1 wires, this initial structure of A3 wire is not stable. The structural optimization starting from this planar geometry yield either A3 wire shown in Fig. 4 or two separate weakly interacting A1 nanowires. When the planar geometry is constrained during the optimization, the structure is transformed into two separated A1 structures. However, the former is energetically more favorable than the latter. The structures of A4 and A5 wires resemble to each other. In the A5 structure, one of the in-plane O pairs, namely O(2) and O(3), has been rotated by 90° with respect to the other in-plane O pair, O(4)

TABLE III. Optimized lattice constant c_0 (in Å), interatomic bond distances d_{1-2}, d_{2-3}, d_{1-3}, d_{1-4}, d_{2-4}, d_{2-5}, and d_{3-5} (in Å), α (in degree), binding energies E_b and E_b^r (binding energy with respect to rutile bulk binding energy) (in eV/f.u.) of $(TiO_2)_n$ nanowires. The energy band gap (in eV) of the semiconducting wires are also reported. E_b of rutile bulk phase is included for comparison. The definitions of E_b and E_b^r are given in the text.

Wire	c_0	d_{1-2}	d_{2-3}	d_{1-3}	d_{1-4}	d_{2-4}	d_{2-5}	d_{3-5}	α	E_b	E_b^r	E_g
A1	3.45	1.64		1.88		3.45			133.6	−17.37	3.14	1.98
A2	6.70	1.65		1.86		6.70			128.1	−17.47	3.04	1.96
A3	3.65	1.64		1.98	1.99				84.5	−18.60	1.91	2.45
A4	2.85	1.89	2.48			2.85			82.1	−17.33	3.17	0.8
A5	5.45	1.85	2.51			3.25			85.4	−19.30	1.20	2.98
A6	8.25	1.86	2.51			3.00			84.7	−18.89	1.62	
A7	11.1	1.87	2.5			2.9			84.2	−18.43	2.06	
A9	6.10	1.85	1.89			2.40		2.49	79.7	−18.44	2.07	2.52
A10	6.35	1.82	1.83		2.55		2.60		88.8	−18.09	2.42	1.33
A11	3.28		1.85		2.48	1.84	2.72		84.6	−19.76	0.74	3.68
Rutile										−20.51	0.00	1.90

and O(5). When one O pair [e.g., O(2)–O(3)] of the A4 wire has been slightly rotated, the disturbed wire transforms into the A5 wire upon relaxation of the perturbed structure. There is no energy barrier from A4 structure to A5 wire. The distance between two O atoms, namely 2 and 4, (d_{2-4}) in A4 and A5 structures is 2.85 and 3.25 Å, respectively. Therefore, the repulsive interaction strength between O pairs in A5 is lower than that in A4. Hence, binding in A5 wire enhances, where A5 wire is 3.94 eV more energetic than the A4 structure. Cluster model of the A5 structure have been studied previously.[44] At each end of the cluster, the monovalent O atoms bind to the Ti atoms in an antisymmetrical manner. E_b per f.u. increases with increasing number of TiO_2 units. Therefore, infinite A5 wire is the upper limit of E_b in these cluster model of A5 wires.

We have also formed the helical structures (A6, A7, and A8) from A4 wire in order to investigate the relative stability of A4 and A5 structures. Each O pair has been rotated with respect to nearest O pairs with a rotation angle δ of 60° in A6, 45° in A7 and 36° in A8 structure as seen in Fig. 4. The distance d_{2-4} in A6, A7, and A8 wires is longer than that in the A4 structure. The distance d_{2-3} affects the coupling between the in-plane O atoms. When it is compared within the series of A4 to A8 wires, the value of d_{2-3} starts to decrease from A5 and reaches its minimum value at A4 wire. So, it is the longest (shortest) in the A4 (A5) structure. Bond lengths d_{1-2} and d_{2-3} in A6, A7, and A8 wires are between d_{1-2} and d_{2-3} of the A4 and A5 wires. Therefore, helical structures are energetically more stable than A4. E_b reaches its maximum value when δ=90°. E_b of these helical structures are between those of A4 and A5. While A4 wire sets the lower limit of E_b, upper limit of E_b occurs at A5 structure. A8 structure does not preserve the initial helical structure and tends to change its structure to A5. Hence, as a result of structural optimization, we have obtained an irregular helical structure for this case.

Coordination number of Ti atoms also strongly influences the binding of nanowires. Binding increases with increasing coordination of Ti atoms. For example, in A2 and A4 geometries, the coordination number of Ti is three and four, respectively. Coordination number also changes the bond lengths, the bond lengths increase when the coordination number of atoms increases. When the monovalent O atoms in the A1 and A2 structures are removed, one obtains the TiO zigzag chain presented in Fig. 1. Due to the monovalent O atom, d_{1-3} in A1 is 2.7% longer than d_{1-2} in TiO zigzag wire. The bond angle α in A1 is 2.2% smaller than the bond angle in TiO zigzag structure. Consider the B3 wire formed upon removal of the monovalent O atoms of the A2 structure. The lattice constants of B3 and A2 structures differ only by 0.1 Å. Energy gain E_{gain} of B3 wire at equilibrium upon adsorption of two O atoms can be calculated with the following formula: $E_{gain}=(E_T[\mathrm{A2}]+2E[\mathrm{O}]-E_T[\mathrm{B3}])$. $E_T[\mathrm{A2}]$ and $E_T[\mathrm{B3}]$ are the total energies of A2 and B3 wires at c =6.6 Å. The energy gain upon adsorption of two O atoms to Ti atoms (atom 1 and atom 3 shown in Fig. 1) in B3 wire is 14.51 eV. $(TiO_2)_n$ and $(TiO)_n$ wires can be transformed into each other by adding or removing O atom. However, Ti and O atoms tend to reach the sufficient coordination number to support their formal oxidation states. Therefore, $(TiO)_n$ wires gain huge energy upon adsorption of O atoms.

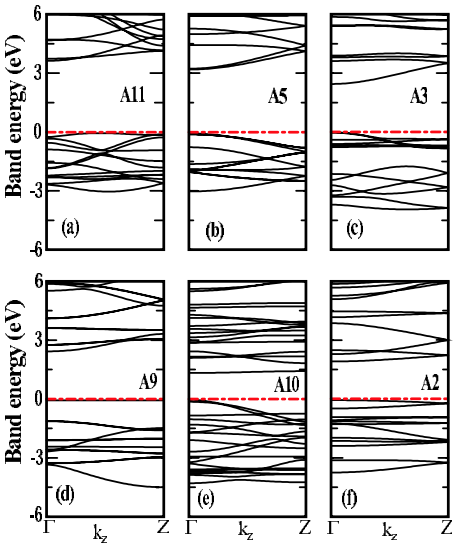

FIG. 6. (Color online) The band structure of the selected $(TiO_2)_n$ nanowires. Fermi level of these semiconductor wires are shown by dashed lines mark the zero of energy which indicates the top of the valence band.

In general, TiO_2 nanowires tend to form 3D structures. Planar structures have relatively lower binding energy than 3D structures. Compared to the other wires, the energy of the wire does not change so much upon compression or stretching of A1, A2, A3, and A11 wires as seen in Fig. 5, and similarly B5, B6, and B7 TiO nanowires as depicted in Fig. 2. Variation in E_b with respect to the lattice constant c along the wire axis is wider and shallower for these wires. In the A5 case, the distance between O(2) and O(3) [or O(4)–O(5)] atoms decreases, while wire is being pulled along the z axis. As a result of the increase in the repulsive O–O interaction during stretching, E_b rises rapidly compared to A3 or A11. Magnetic properties have also been investigated for all wire geometries. All studied wires have nonmagnetic ground state in their equilibrium structures.

Electronic properties of $(TiO_2)_n$ wires are explored by band structure calculations, and the relation between electronic properties and stability of these wires is investigated. Electronic band structures of some selected nanowires are presented in Fig. 6. As inferred from Fig. 6, all studied $(TiO_2)_n$ nanowires are semiconductors. Energy band gaps, E_g, range from 0.8 to 3.68 eV compared to the 1.90 eV calculated band gap of bulk rutile. There is a direct correlation between E_g and E_b. In general, E_g increases with increasing E_b. We have examined in detail how the band structures are modified between similar structures [(A1, A2, A3) and (A4, A5)]. For example, there is a dramatic differences between the band structures of A4 and A5 wires. In the A4 structure, the band gap has indirect nature and the value of E_g is about 0.8 eV. E_g is about 2.98 eV for A5 wire, moreover its character is changed to a direct band gap. Remember that E_b of A5 is 1.97 eV lower than the one of A4 wire. The band-gap behavior with different rotation angles, δ, of one of the O pair (see Fig. 4) of A4 or A5 wire is studied in detail and is presented in Fig. 7. The equilibrium structure of A5

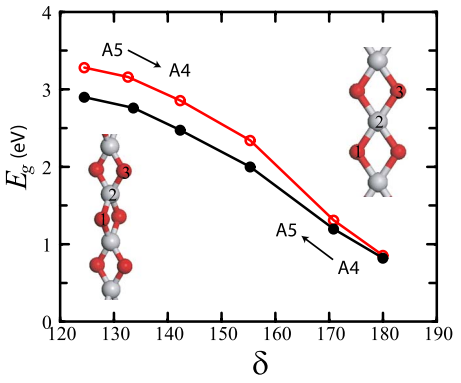

FIG. 7. (Color online) Variation in band gap E_g of A4 and A5 wires with the rotation angle δ which is the angle among O1–T2–O3 atoms (see Fig. 4).

(A4) is taken, and one of the O pair is rotated gradually ending up in the A4 (A5) structure. Electronic band structure calculations are carried out without relaxing the modified structures. Doubled unit cell is used for the calculations of the A4 structure for direct comparison with the A5 results. This way, as displayed in Fig. 7, two different E_g versus rotation angle δ curves are resulted depending on the path, i.e., starting from A5 structure and ending with A4 wire or vice versa. E_g's of these rotated structures are between those of A4 and A5 wires. E_g decreases from A5 to A4. Hence, electronic structure is very sensitive to rotation, elongation, and contraction in the A4 and A5 structures. So, it is possible to tune the electronic properties of these wires by applying tension.

A1 and A2 structures have similar electronic band structures. Nature of the band gap is direct. E_g of A1 and A2 is 1.98 and 1.96 eV, respectively. A3 is more stable than A1 and A2. Hence, it is expected that it has a relatively large E_g, which is calculated as 2.45 eV. A11 structure is the most stable structure. Its E_g is 3.68 eV and the band gap is indirect. In $(TiO_2)_n$ wires, Ti and O atoms have $10(p^6d^3s^1)$ and $6(s^2p^4)$ valence electrons, respectively. Ti atoms donate their four electrons to two O atoms to fill the unoccupied states of O atom. This behavior causes the semiconductor nature of $(TiO_2)_n$ wires.

Stoichiometric and nonstoichiometric thin Ti–O wires can be formed on TiO_2 surfaces upon reconstruction or annealing. Therefore, it is important to understand structural, magnetic, and electronic properties of these nanowires. Unlike stoichiometric TiO_2 nanowires, Ti_2O_3 quasi-one-dimensional chains formed on reconstructed rutile [110] surface exhibit metallic behavior.[8] Moreover, we have both metallic and semiconducting $(TiO)_n$ nanowires. As a result, it is expected that stoichiometry strongly influences the electronic properties of Ti–O nanowires.

C. Bulklike rutile (110) nanowires

Finally, we have studied the structural and electronic properties of bulklike TiO_2 nanowires. We considered bulklike rutile (110) nanowires, since, recently these wires are experimentally realized and synthesized.[11] The nanowires

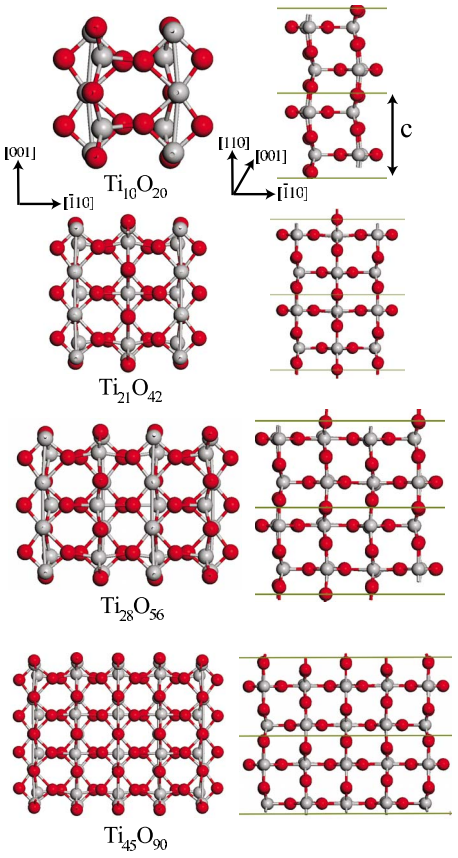

FIG. 8. (Color online) Top and side view of the optimized geometric structure of the bulklike TiO_2 nanowires extended along the rutile [110] direction. Grey and red balls are used to represent the Ti and O atoms, respectively.

studied here have been cut in rodlike forms from the ideal bulk rutile crystal. Nanowires are oriented along the rutile [110] crystallographic direction and each nanowire has different diameter. All of them have rectangular cross-section and they have two (110) and (001) lateral surfaces. It is known that (110) surface is the most stable surface among the rutile surfaces. Figure 8 shows the optimized structure of some of these nanowires. We have calculated the E_b of these 1D structure as a function of number of TiO_2 units. It is important to figure out how the stability and electronic properties of these nanowires evolve as the cross-section changes. The comparison of E_b of A5, A11, and TiO_2 bulklike nanowires is shown in Fig. 9. It is noticed that bulk wires are energetically more stable than A5 structure. However, A11

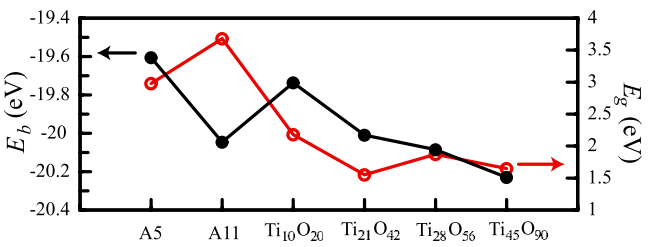

FIG. 9. (Color online) Comparison of the atomically thin and bulklike TiO_2 nanowires. E_b and E_g are given in eV.

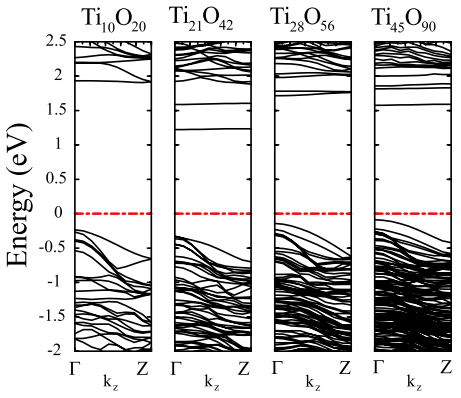

FIG. 10. (Color online) The band structure of the various bulklike rutile (110) nanowires. Fermi level is represented by dotted-dashed lines.

structure is slightly more stable than $Ti_{10}O_{20}$ and $Ti_{21}O_{42}$ nanowires. There is a crossover after the $Ti_{21}O_{42}$ nanowire, and the bulk wires with larger radius than this nanowire become more energetically stable. Internal regions of $Ti_{28}O_{56}$ and $Ti_{45}O_{90}$ nanowires exhibit more bulklike behavior. Rutile phase is 0.5 eV more energetic than $Ti_{45}O_{90}$ nanowire. Structural distortion of initial structure of bulklike wires upon geometry optimization decreases as the cross-section increases. In Fig. 10, we have shown the band structure of these rutile (110) nanowires. Bands around the Fermi level E_F has mainly O $2p$ character. The lowest conduction bands are very flat and has d character. Except $Ti_{10}O_{20}$, all nanowires have direct gap. In $Ti_{10}O_{20}$ case, indirect energy gap is slightly smaller than direct one. E_g of these nanowires is displayed in Fig. 9. E_g shows an oscillation around 1.75 eV which is close to theoretical E_g of bulk rutile.

IV. CONCLUSIONS

In summary, structural, electronic and magnetic properties of atomically thin TiO_x $(x=1,2)$ and bulklike rutile (110) nanowires have been investigated from first-principles calculations based on DFT. All stoichiometric thin TiO_2 nanowires are semiconductors and have paramagnetic ground state. It has been found that there is a strong correlation between E_g and E_b of these TiO_2 nanowires. To gain the more insight about the relative stability of the atomically thin stoichiometric TiO_2 nanowires, we have also studied the bulklike rutile (110) nanowires, which are cut in a rodlike structure from crystalline rutile bulk and oriented along the [110] crystallographic direction. These bulklike nanowires become energetically more stable with respect to thin nanowires after a certain cross-section, and all of them are semiconductors. E_g of these thick nanowires oscillates around the computed E_g of bulk rutile. Nonstoichiometric thin TiO wires have been also studied. They exhibit various electronic and magnetic properties. There are both metallic and semiconducting wires. Unlike stoichiometric titania nanowires, some of the TiO wires have magnetic ground state.

ACKNOWLEDGMENTS

Part of the calculations has been carried out at ULAKBIM Computer Center and UYBHM at Istanbul Technical University. O.G. acknowledges the support of Turkish Academy of Sciences, TÜBA.

*gulseren@fen.bilkent.edu.tr

[1] U. Diebold, Surf. Sci. Rep. **48**, 53 (2003).
[2] T. L. Thompson and J. T. Yates, Jr., Chem. Rev. (Washington, D.C.) **106**, 4428 (2006).
[3] X. Chen and S. S. Mao, Chem. Rev. (Washington, D.C.) **107**, 2891 (2007).
[4] G. Wang, Q. Wang, W. Lu, and J. Li, J. Phys. Chem. B **110**, 22029 (2006).
[5] B. Tan and Y. Wu, J. Phys. Chem. B **110**, 15932 (2006).
[6] J. Jiu, S. Isoda, F. Wang, and M. Adachi, J. Phys. Chem. B **110**, 2087 (2006).
[7] S. P. Albu, A. Ghicov, J. M. Macak, R. Hahn, and P. Schmuki, Nano Lett. **7**, 1286 (2007).
[8] M. Blanco-Rey, J. Abad, C. Rogero, J. Mendez, M. F. Lopez, J. A. Martin-Gago, and P. L. de Andres, Phys. Rev. Lett. **96**, 055502 (2006).
[9] B. Yilmaz, J. Warzywoda, and A. Sacco, Jr., Nanotechnology **17**, 4092 (2006).
[10] B. Yilmaz, A. Sacco, Jr., and J. Deng, Appl. Phys. Lett. **90**, 152101 (2007).
[11] S. S. Amin, A. W. Nicholls, and T. T. Xu, Nanotechnology **18**, 445609 (2007).
[12] B. Poudel, W. Z. Wang, C. Dames, J. Y. Huang, S. Kunwar, D. Z. Wang, D. Banerjee, G. Chen, and Z. F. Ren, Nanotechnology **16**, 1935 (2005).
[13] C. Liu and S. Yang, ACS Nano **3**, 1025 (2009).
[14] A. Damin, F. X. L. Xamena, C. Lamberti, B. Civalleri, C. M. Z. Wilson, and A. Zecchina, J. Phys. Chem. B **108**, 1328 (2004).
[15] A. N. Enyashin, V. V. Ivanovskaya, Y. N. Makurin, V. G. Bamburov, and A. L. Ivanovskii, Dokl. Phys. Chem. **391**, 187 (2003).
[16] A. N. Enyashin and G. Seifert, Phys. Status Solidi B **242**, 1361 (2005).
[17] D. Zhang, P. Liu, and C. Liu, J. Phys. Chem. C **112**, 16729 (2008).
[18] H. Peng and J. Li, J. Phys. Chem. C **112**, 20241 (2008).
[19] M. C. Payne, M. P. Teter, D. C. Allen, T. A. Arias, and J. D. Joannopoulos, Rev. Mod. Phys. **64**, 1045 (1992).
[20] Numerical computations have been carried out by using VASP software: G. Kresse and J. Hafner, Phys. Rev. B **47**, 558 (1993); G. Kresse and J. Furthmüller, *ibid.* **54**, 11169 (1996).
[21] W. Kohn and L. J. Sham, Phys. Rev. **140**, A1133 (1965); P. Hohenberg and W. Kohn, *ibid.* **136**, B864 (1964).
[22] D. Vanderbilt, Phys. Rev. B **41**, 7892 (1990).
[23] P. E. Blöchl, Phys. Rev. B **50**, 17953 (1994).
[24] G. Kresse and D. Joubert, Phys. Rev. B **59**, 1758 (1999).
[25] J. P. Perdew and Y. Wang, Phys. Rev. B **45**, 13244 (1992).
[26] H. J. Monkhorst and J. D. Pack, Phys. Rev. B **13**, 5188 (1976).

[27] M. Methfessel and A. T. Paxton, Phys. Rev. B **40**, 3616 (1989).
[28] S. C. Abrahams and J. L. Bernstein, J. Chem. Phys. **55**, 3206 (1971).
[29] J. K. Burdett, T. Hughbanks, G. J. Miller, J. W. Richardson, Jr., and J. V. Smith, J. Am. Chem. Soc. **109**, 3639 (1987).
[30] C. J. Howard, Z. M. Sabine, and F. Dickson, Acta Crystallogr., Sect. B: Struct. Sci. **47**, 462 (1991).
[31] S. J. Thompson and S. P. Lewis, Phys. Rev. B **73**, 073403 (2006).
[32] A. Kiejna, T. Pabisiak, and S. W. Gao, J. Phys.: Condens. Matter **18**, 4207 (2006).
[33] S. P. Bates, G. Kresse, and M. J. Gillan, Surf. Sci. **385**, 386 (1997).
[34] T. Bredow, L. Giordano, F. Cinquini, and G. Pacchioni, Phys. Rev. B **70**, 035419 (2004).
[35] F. Labat, P. Baranek, and C. Adamo, J. Chem. Theory Comput. **4**, 341 (2008).
[36] H. Perron, C. Domain, J. Roques, R. Drot, E. Simoni, and H. Catalette, Theor. Chem. Acc. **117**, 565 (2007).
[37] H. Tang, F. Levy, H. Berger, and P. E. Schmid, Phys. Rev. B **52**, 7771 (1995).
[38] A. V. Emeline, G. V. Kataeva, V. K. Ryabchuk, and N. Serpone, J. Phys. Chem. B **103**, 9190 (1999).
[39] K. P. Huber and G. Herzberg, *Molecular Spectra and Molecular Structure* (Van Nostrand Reinhold, New York, 1979), Vol. IV.
[40] N. S. McIntyre, K. R. Thompson, and W. Weltner, Jr., J. Phys. Chem. **75**, 3243 (1971).
[41] D. Watanabe, J. R. Castles, A. Jostsons, and A. S. Malin, Acta Crystallogr. **23**, 307 (1967).
[42] C. Leung, M. Weinert, P. B. Allen, and R. M. Wentzcovitch, Phys. Rev. B **54**, 7857 (1996).
[43] J. Graciani, A. Márquez, and Javier Fdez. Sanz, Phys. Rev. B **72**, 054117 (2005).
[44] K. S. Jeong, C. Chang, E. Sedlmayr, and D. Sülze, J. Phys. B **33**, 3417 (2000).